Additive Manufacturing Letters 9 (2024) 100193

Contents lists available at ScienceDirect

Additive Manufacturing Letters

journal homepage: www.elsevier.com/locate/addlet

Short Communication

Vat photopolymerization additive manufacturing process modeling: a thermal-chemical coupling approach informed by in-situ and ex-situ characterization data

Heyang Zhang, Yue Zhang, Xiayun Zhao *

Department of Mechanical Engineering and Materials Science, University of Pittsburgh, Pittsburgh, PA 15261, USA

ARTICLE INFO

Keywords:
Additive manufacturing
Vat photopolymerization
Degree of conversion
In-situ monitoring
Photo differential scanning calorimetry

ABSTRACT

Vat photopolymerization (VPP) is one of the most widely used additive manufacturing methods. The VPP process temperature and material curing reaction interplay with each other to critically determine the final product quality. Insights about the time-varying process temperature and degree of conversion (DoC) is desired for VPP process control but difficult to attain due to lacking effective operando characterization technologies. This work reports a new method to create a thermal-chemical model of the VPP process by solving an inverse heat conduction problem (IHCP) based on in-situ observable temperature measurement to estimate the chemistry reaction-induced heat source that is a function of DoC. Ex-situ photo differential scanning calorimetry (Photo-DSC) characterization is used to initialize the chemistry reaction model parameters so that DoC can be calculated. Specifically, vat substrate temperature is measured using an in-situ infrared thermal camera and used as input to solve an IHCP for estimating exothermic heat generation rate for the internal heat generation component at the curing part. Overall, the newly developed VPP modeling framework combines an IHCP that is optimized by in-situ thermal monitoring with a chemical reaction heat generation and conduction model that is educated by Photo-DSC characterization. The model predictions of temperature and DoC are experimentally validated by comparing against in-situ temperature measurement and ex-situ spectroscopy measurement of prints at different exposure times.

1. Introduction

1.1. Vat photopolymerization, temperature, and degree of conversion

Vat photopolymerization (VPP) is an additive manufacturing (AM) process in which liquid photopolymers are selectively cured using light-activated polymerization to create a desired 3-D part layer by layer [1]. VPP-based AM mainly uses ultraviolet (UV) light and visible light to initiate the photopolymerization of precursor liquid resin [2,3] and finds great applications in commercial manufacturing, medicine, dentistry, automobile industry, and aviation [4–6]. One way the light is delivered is through digital light processing (DLP), in which light emitting diode (LED) signals are shaped using digital micromirror devices (DMD) to create a 2-D optical mask corresponding to a cross-section profile of the desired 3D part [7]. This allows the resin to be cured one layer at a time, as opposed to one voxel at a time as in processes like stereolithography (SLA). A simplified representation of the VPP process is shown in Fig. A-1.

The photopolymerization reactions in the VPP process are usually exothermic and could cause spatiotemporal changes in temperature within the curing zone. As the VPP processing temperature is dominated by the heat from chemical reactions, it would in turn affect the reaction kinetics, resin viscosity, and part properties [8,9]. It would be of great interest to know the temperature due to the exothermic reactions in VPP to understand the VPP process-structure-property. Meanwhile, the VPP material behavior is typically evaluated by the degree of conversion (DoC), which critically determines the geometrical and mechanical properties. For instance, undercuring could be detrimental to the mechanical strength while overcuring could negatively affect the geometric accuracy [10–12].

Recent works have shown the feasibilities of dual-material systems that can be cured at different wavelengths, which allows for printing of multi-material parts in parallel to create products with different material properties [10,13,14]. The increased complexity of a dual-material and

* Corresponding author.
E-mail address: xiayun.zhao@pitt.edu (X. Zhao).

https://doi.org/10.1016/j.addlet.2024.100193
Received 3 October 2023; Received in revised form 22 December 2023; Accepted 10 January 2024
Available online 13 January 2024

dual-reaction system, even without considering the increased complexity of the system, means for doubling the control difficulty and greater tendency to incur print errors. With the dual-material systems still in its infancy, most of the work done in literature is in extremely controlled lab environments. One major problem, often downplayed, is the extremely long layer cure time in the magnitude of minutes, that is required for the one-pot resins [10]. In addition, the layer cure time for the different materials is dependent on the material system as well as the intensity of the different wavelengths of light. As such, it is vital to ensure the consistent degree of cure of both desired materials. Instead of the common method of experimental trials to determine exposure times, an approach to model the distribution and variation of temperature and DoC during the multi-material VPP can be used instead [15].

1.2. Modelling vat photopolymerization

Models of photopolymerization have been explored in depth in the chemistry field, however application of such is lacking in the context of VPP. Prediction models coupling temperature with degree of cure, such as that of Goodner et al., create curing kinetic model of free-radical polymerization with mass and heat transfer based on polymerization models and glass transition temperatures [16,17]. The developed model is then used to estimate the values of temperature and conversion as a function of both time and depth in a polymerization system. However, the extensive work, while elaborate, is heavily experimental parameter driven, in which the material specific reaction coefficients need to be well measured. Furthermore, the prediction model does not consider the geometry and unique printing set-up of VPP printer vats, which could cause variations in the size of surfaces exposed to light and oxygen.

The theoretical feasibility of the creation of chemical-mechanical-thermal VPP model was shown in the work of Classen et al. [18]. However, the work was done on a 1-dimension hypothetical model. Further studies need to be done to transition this work into real-world applications. Yet, work on chemical-mechanical models of VPP has been done to study the geometric accuracy of the printed product [19–21]. Through the use of tokens, models are able to predict shrinkage and deformation of the printed product due to the stress-strain of the polymerization process. However, the model assumes an isothermal state and a constant rate of reaction, which causes accuracy issues to the chemical model of the presented work [19]. Many existing works have been modelling on a chemical mechanism level for estimating the curing reactions during VPP printing [20,21]. The targeted application of these models is mainly on achieving part geometry accuracy through controlling the input of optical exposure profile and thus regulating the reactions. However, these studies usually use basic monomers and rely heavily on literature for acquiring the plethora of model parameters that are needed to build a complete chemical model. The commonly used approach cannot create an accurate model since the material is subject to batch-to-batch variations and the model parameters could also vary in realistic printing processes that tend to fluctuate as well. The research currently available highlights the difficulty of a robust model of the VPP process that includes an insightful and practical chemical model which could reflect the real material properties and process conditions.

Overall, accurate and robust methods of modelling the chemistry is greatly needed to advance VPP for sophisticated applications that demand localized property control in cases such as metamaterials and soft robots. Especially, the modelling method need to be flexible to the rapid rise of new materials without the need for extensive material property studies. This work aims to leverage exothermic heat signals as a method of observation to fine tune a data-driven heat source function to model the chemistry of VPP printing of a simple sample. The work discussed can be then further leveraged to model more complex geometries.

1.3. Photo differential scanning calorimetry for thermal and DoC analysis in VPP

Photo differential scanning calorimetry (Photo-DSC) is an analytical technique to study the thermodynamic and material properties in light-induced processes by measuring the heat output of reactions in closed and controlled temperature environments [22]. As the VPP printing is fundamentally a chemical photopolymerization process, Photo-DSC has been used to an extent to study the thermal and chemical properties of the material systems, namely heat capacity and heat of polymerization [23–27]. Furthermore, Photo-DSC has been applied to more complex materials that allow for dual curing printing to study how material properties are effected by temperature [28]. The use of Photo-DSC to measure reaction enthalpy and calculate DoC in VPP, however, has come under scrutiny for its lack of consistency and scalability due to the significant differences in terms of material geometry, volume and processing between in a crucible and in a VPP printer [29].

While recognizing the limitations of Photo-DSC as a method for studying VPP materials, in this work we use Photo-DSC characterization to gain a preliminary understanding of a VPP material system and obtain a good set of initial values of the parameters for optimizing a model that correlates the process temperature with the DoC of VPP printed parts.

1.4. The inverse heat conduction problem (IHCP)

The difficulties of measuring the temperature at relevant regions during the VPP process have been highlighted during works examining temperature effects [9]. This is especially heightened in a bottom-up system, in which the region of interest – the areas of the resin undergoing curing, is typically not accessible for infrared (IR) observations [30]. Such a problem can be as an inverse heat conduction problem (IHCP), which has found applications in a range of engineering fields from metallurgy, aerospace, and material processing [31]. Fundamentally, IHCP is an ill-posed problem that is extremely sensitive to measurement errors [32]. Attempts to overcome this issue has found success via Duhamel's theorem, specified sequential function method, regularization method, transfer function method, and more recently, the use of convolutional neural networks, long short-term memory networks, and a combination of these methods [32–35]. These methods, however, are applied to thermal problems with open boundary conditions.

1.5. Gaps and objectives

Noticeably, exploration into thermal-based simulations of VPP geometries has been lacking – especially in leveraging the exothermic chemistry of the curing process. Furthermore, although work has been done in investigating IHCP's that involve unknown transient heat sources, the idea to couple chemistry induced exothermic heat sources to constrain the problem has not been maturely explored. As such, this work aims to predict the temperature profile of a curing zone and the bulk DoC of the corresponding VPP-printed part by measuring the transient temperature distribution of the vat's exterior bottom surface and applying the signal to an IHCP algorithm to optimize for the exothermic reaction rate model, and as such predict the DoC during VPP.

The remainder of this paper is organized as follows. The experimental setup of the in-situ temperature measurement and ex-situ characterization will be described in Section 2. The methods of IHCP will also be introduced in Section 3 by first exploring the forward heat conduction problem, and then the optimization of the parameters of the forward problem to solve the IHCP. The results of the IHCP are then presented in Section 4, where the predicted DoC and temperature are compared and validated against experimental measurements.

2. Material and methods

2.1. Overview and experiment design

The overall framework comprises the following methods. The in-situ thermal measurements and DoC data of one sample (e.g., a sample cured with 30 second exposure time) is used as the input of an IHCP optimization algorithm to fine tune the chemical-thermal model. The IHCP model is made up the forward heat transfer problem of the geometry of the print vat, with an internal heat source modelled using polymerization models. The appropriate model is selected based on ex-situ photo-DSC results of the material system. Similarly, the initial guesses of the optimization algorithm, which aim to minimize the effects of local minima, are also educated by photo-DSC results of the material system.

Acting as a preliminary study, this work considers a bulk VPP curing to reduce the complexity such as the effect of resin flow on heat transfer during multi-layer VPP and the computational expense due to increased complexity of multi-layer geometry. Therefore, multiple one-layer samples are printed at a range of exposure times (20, 30, 40, 50 s). The corresponding VPP process is monitored by a thermal camera capturing the temperature of the bottom of the resin vat. It is important to note that the vat is left to rest and returns back to room temperature between each trial. Nevertheless, the framework of the curing in VPP process developed in this work paves the way for further study on a chemical-thermal VPP model, and in turn a true multi-physical model in the future.

The appendix Fig. A-1 shows the DLP based VPP printer that we used in this experiment. A circular mask of diameter 5.42 mm was projected into the resin with a targeted thickness of 3 mm to be printed using a blue light (460 nm) at 5.74 mW/cm^2 and UV light (360 nm) at 23.06 mW/cm^2. The resin was continuously cured for 10, 20, 30, 40, and 50 s for two trials while the thermography of the bottom of the resin vat was observed and recorded. The DoC of the printed parts were then measured using Fourier transformed infrared (FTIR) spectroscopy as detailed in Section 2.4.

2.2. Material system

A more challenging dual-curing material system is used in this work to demonstrate the potential applicability of the proposed method for evaluating chemical and thermal behaviors of both traditional single-wavelength single-material VPP and emerging multi-wavelength multi-material VPP. The material system used in the presented work comprises an epoxy-based group that can be cured by UV light and an acrylate-based group that can be cured by both UV and blue lights. Acrylate and epoxy monomers and their corresponding initiators constitutes the two-wavelength responsive, multi-component system, which is adapted from the system used by Schwartz et al. [10]. The material system was made up of 50 wt% Glycidyl methacrylate (GMA) and 50 wt % Ethylene glycol dimethacrylate (EGDMA). 2.5 wt% Irgacure 819 was selected as the free radical initiator, and 2.5 wt% triarylsulfonium salts solution (TAS, obtained and used as a 50 wt% solution in propylene carbonate) used as the cationic initiator, and weight precent of initiators was based on total monomers. Under UV light, both TAS and Irgacure 819 will be activated to cure the epoxy groups in GMA and the acrylate groups in GMA and EGDMA, respectively, to create a stiff material. Under visible light, only Irgacure 819 will be activated to cure the acrylate components to provide a soft material. All materials were sourced from Sigma Aldrich.

The vat substrate made with TEFLON fluorinated ethylene propylene (FEP) film is used for its high temperature resistance, good mechanical resistance, and oxygen permeability. Work has shown that it can create an oxygen inhibition zone to prevent the adhesions between cured part and the film [36].

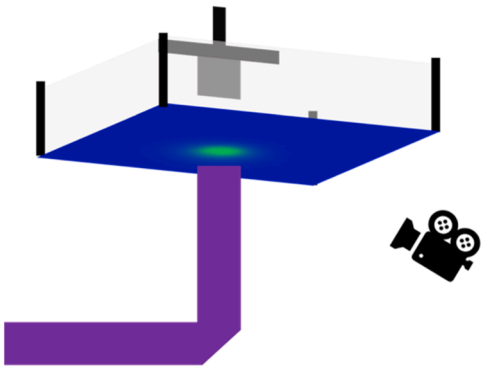

Fig. 1. Thermal camera setup for in-situ monitoring during DLP print.

2.3. In-situ thermal monitoring

An in-situ temperature monitoring protocol to measure the reachable surface temperature is developed in our previous work [30]. Specifically, in this work, a thermal camera (FLIR ThermaCAM S40) is installed under the vat at a 25-degree angle from the surface of the vat and pointed at the bottom of the resin chamber, shown in Fig. 1. The angle is set limited based on the printer construction and the curing light path into the vat.

A perspective transformation is conducted using a custom metal plate with four square holes to calibrate the geometry of acquired thermal images of vat bottom surface. The calibration can be seen from Fig. 2(a) to Fig. 2(b).

Furthermore, due to the radial symmetry of the circular samples printed in this work, the same symmetry is expected in the thermal distribution. Therefore, the radial temperature is extracted by finding the location of the maximum temperature and assuming it to be the origin of the radial distribution, as shown in the dotted line in Fig. 3(a). An example of the measured radial temperature profile of vat bottom surface is shown in Fig. 3(b) with each line representing the distribution at a time step. These in-situ measurements are the input to the IHCP based model optimization and simulation to be discussed in Section 3.2.

2.4. Validation of the predicted DoC via ex-situ ftir spectroscopy characterization

A FTIR spectroscopy (Vertex-70LS, Bruker, Billerica, MA) is used to measure the DoC ex-situ for validating the predicted DoC at different exposure times. The absorption spectrum is measured by performing 16 scans with a resolution of 4 cm^{-1} in attenuated total reflection (ATR) mode, and then taking the average of the results. Then DoC is calculated as the conversion of the aliphatic C=C bond peak at the peak frequency 1638 cm^{-1}. The stable C=O stretch peak at peak frequency 1725 cm^{-1} is used as the internal reference. The ratio of $\frac{\text{C=C bond peak area}}{\text{C=O bond peak area}}$ of the cured sample and unreacted resin was measured. The DoC is calculated using the ratio of peak area as shown in Eq. (1).

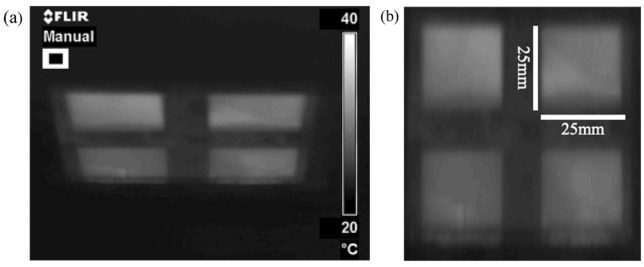

Fig. 2. Perspective transformation calibration of off-axis thermal camera. (a) pre-calibration (b) post-calibration.

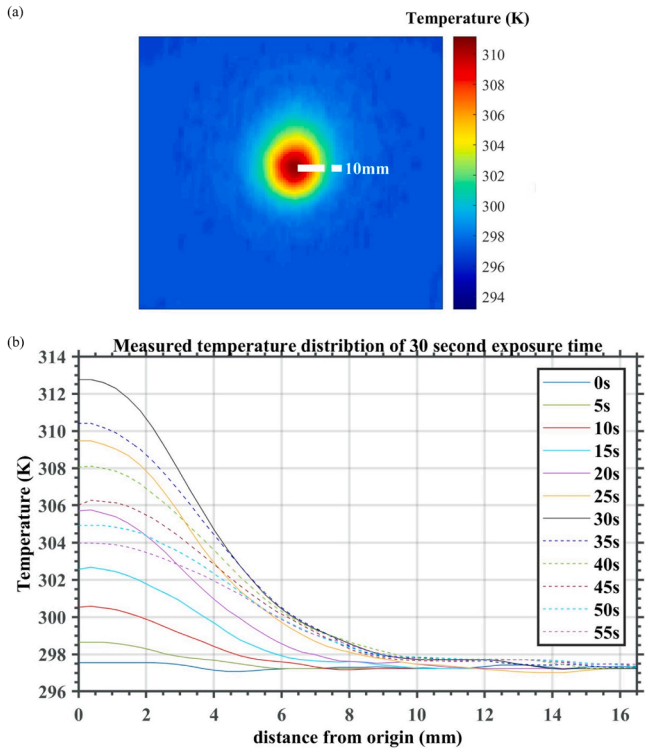

Fig. 3. (a) Sample raw data collected through thermography; (b) Radial line profile of vat substrate temperature extracted for IHCP optimization.

$$DoC_{FTIR} = 1 - \frac{(A_{1638}/A_{1725})_{cured\ sample}}{(A_{1638}/A_{1725})_{resin}} \tag{1}$$

where A_{1638} is the peak area of aliphatic C=C bond peak and A_{1725} is the peak are of stable C=O stretch peak. An example FTIR measurement of the DoC of a sample cured for 30 s, which is used in the model optimization in Section 4.2, is shown in the appendix Fig. A-3.

3. Theory

3.1. The forward problem: chemical reaction heat conduction finite-element model of VPP

The application of an inverse heat conduction problem starts with a forward heat conduction model. The model is based on the solid thermal conduction equation shown in Eq. (2). The photopolymerization process in VPP can be described with a heat generation term, q_{active}, caused by the exothermic heat generated during the chemical reactions. The q_{active} heat source geometrically is a subset of the resin geometry.

$$\frac{\partial^2 T_{resin}}{\partial r^2} + \frac{1}{r}\left(\frac{\partial T_{resin}}{\partial r}\right) + \frac{\partial^2 T_{resin}}{\partial z^2} + \frac{q_{active}}{k} = \frac{1}{\alpha}\frac{\partial T_{resin}}{\partial t} \tag{2}$$

The heat generated is associated with the rate of cure, $\frac{d\alpha}{dt}$, (where α is the degree of conversion), scaled by the change in enthalpy, ΔH. This relationship is detailed in Eq. (3) [23]. Note that the printing zone where exothermic reactions take place serves as a heat source that releases certain amount of heat, q_{active}, which depends on the DoC and in turn will affect the temperature profile in the printing material system.

$$q_{active} = \text{Heat Production Rate} = -\Delta H\left(\frac{d\alpha}{dt}\right) \tag{3}$$

The rate of cure, $\frac{d\alpha}{dt}$, is the main factor in this heat production model and is dependent on the chemical reaction model of polymerization of the resin. The model used in this work is detailed in Eq. (4).

$$\frac{d\alpha}{dt} = \Lambda e^{\frac{-E}{RT}}(1-\alpha)^n(\alpha)^m \tag{4}$$

In Eq. (4), the rate of reaction, $\frac{d\alpha}{dt}$, is defined by the concentration of the monomer, $(1-\alpha)$, and the concentration of the product, α, which is also defined as the DoC of the reaction. The rate of reaction is scaled by the pre-exponential factor, Λ, and the temperature dependent Arrhenius factor, $e^{\frac{-E}{RT}}$.

Herein, based on the work done in a previous study [30], COMSOL is used to solve the finite element model (FEM) of thermal dynamics in the VPP process for evaluating the chemical curing process by combining the system equations (Eqs. 2-4). For simplification, the model only assumes the impact of solid heat conduction. Outside the scope of this study, further extension of this work can be made for thermal convection and species transport simulation with extended application of liquid models. To accelerate the simulation, an axisymmetric assumption is made since the printed part is a cylinder. The geometry is shown in Fig. 4, where the axis of symmetry is assigned to be at $x = 0$. The simulation geometry is consisting of three zones based on the printing setup described in Sections 2.1, 2.2, and Appendix A-1: (1) a thin FEP film layer at substrate; (2) a layer of the bulk material system on top of the vat as the inactive (uncured) resin.; and (3) an active region of the material system, occupying the region of the resin that is being cured, to act as the heat source of the thermal model, where q_{active} is applied.

A thermal insulation boundary condition is used in all outward facing surfaces. Assumptions are made for the thermal properties of both the resin and substrate to be invariant relative to temperature. Whilst the model simulation calculates the temperature in the entire 3D axis-symmetrical domain, the main region of interest for the purpose of IHCP is the output of a time curve of temperature profile at the bottom of the vat, corresponding to the in-situ vat bottom surface temperature measurement described in Section 2.3. The comparison of which will act as the basis for the error function for the IHCP optimization discussed in Section 3.2.

3.2. The optimization-based inverse heat conduction problem for VPP process modeling

For addressing the issue pointed out in Section 1.4, in this work, we formulate the VPP process temperature and exothermic heat generation estimation problem as an IHCP by applying in-situ thermography-measured surface temperature as a boundary condition, and imposing chemistry-based fitting parameters to restrict the problem. With the externally measured chemistry kinetics data used as initial values overcoming the local minima, we aim to simplify the IHCP optimization problem such that the problem can be solved with a simplex algorithm. The restricting of the IHCP will be detailed later in this work. It is clear, however, that further extensions could be made such that more general models could be solved by applying the methods to overcome an ill-posed IHCP.

The forward FEM model of chemical reaction heat transfer (Section 3.1) is built using COMSOL with Livelink to MATLAB to allow for the optimization workflow. For the purpose of optimization, one of the 30-second exposure samples was selected as the training data set. The main justification for the selection of the 30-second exposure sample is due to the availability of ground truths for exposure times longer and shorter than the training set. As such, the work can examine the effectiveness of both extracting the DoC history and predicting future DoC trends.

The radial transient temperature of the bottom of the vat substrate, detailed in Section 2.3, is then selected as the output for optimization purposes for the pre-optimized COMSOL simulation model. Root-mean-squared error (RMSE) is calculated between the predicted and measured transient radial substrate temperature. A further constraint of the predicted DoC for this 30-second exposure is compared to the measured results. The RMSE's are weighted such that the order of magnitude

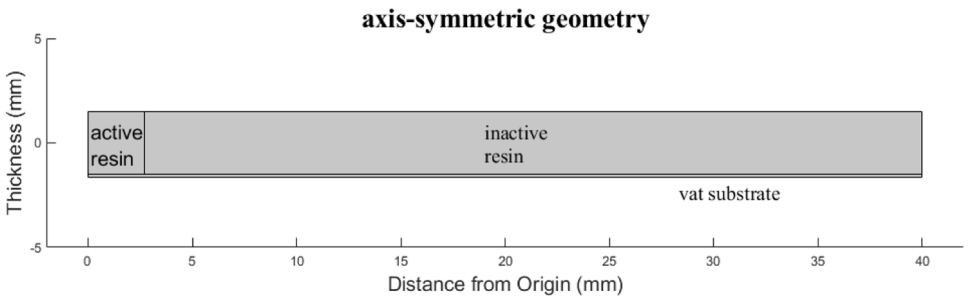

Fig. 4. Geometry of the forward heat conduction model.

between the two RMSE are comparable. This error function is then minimized by controlling the parameters of the reaction rate equation first referenced in Eq. (4). The framework of thermal-chemical modeling of VPP process with the optimization workflow is summarized in *Fig. 5*. The fitting parameter is initialized from the fitting of the Photo-DSC results (Section 4.1). The coefficient parameter and enthalpy, A an ΔH, however, is merged into one coefficient, Λ, in the Photo-DSC result. Thus, the initial fitting values are differentiated to prioritize the accuracy of the model-predicted DoC. The optimization is run using the Nelder-Mead simplex optimization method built in MATLAB. The convergence of the cost optimized is found in Appendix Section A-2.

4. Results and discussions

4.1. Parameter fitting photo-DSC results of material system for IHCP

The main method to address the issue of the ill-defined nature of IHCP in this work is through the use of a well constrained heat source function based on the polymerization model of the material system. As such, initial characterization of the system is done through a series of photo-DSC experiments.

The material system was characterized using a Photo-DSC equipment (NETZSCH model DSC 204 F1) equipped with a Omnicure accessory lamp with a wavelength range of 320–500 nm. Samples were cured in a vacuum-tight inert nitrogen environment until full cure at 5 mW/cm^2 and 10 mW/cm^2 at isotemperatures of 30°C, 40°C, and 50°C.

Examining the raw Photo-DSC data, we can see the evidence of two reactions by the bump at the beginning of the reaction. Two possible explanations of the super-positioning are currently being considered: The curing system of the Photo-DSC, although characterized as mostly UV, has a wide enough spectrum of 320–500 nm to also activate the initiator reactive to blue light at the same time as the UV light, causing both the acrylic and epoxy components to undergo curing reactions; The material system contains two initiators (TAS and Irgacure 819) and two monomers (GMA and EDGMA), leading to acrylic polymerization reactions under the UV and visible exposures

From the current understanding of this material system, the second explanation is more likely and matches up with our observations from the Fourier Transform Infrared (FTIR) characterization of the experimental samples which didn't show that epoxy monomers had been cured. Further exploration of this material system, however, is needed and is outside the scope of this work. Nevertheless, the existence of more than one curing peaks is expected in dual-wavelength curable material system during VPP printing.

Due to availability and resource limitations of the collected photo-DSC data, individual peaks could not be experimentally separated. As such, a gaussian peak separation algorithm is used. The DSC curve is fitted by the sum of two gaussians by minimizing the RMS error is shown to be adequate by the works of Humphry et al. to be used to break up the Photo-DSC data into two Gaussian curves [37,38]. An example of the fitted photo-DSC curve is shown in Fig. 6.

The two Gaussian curves are then fitted using known chemical

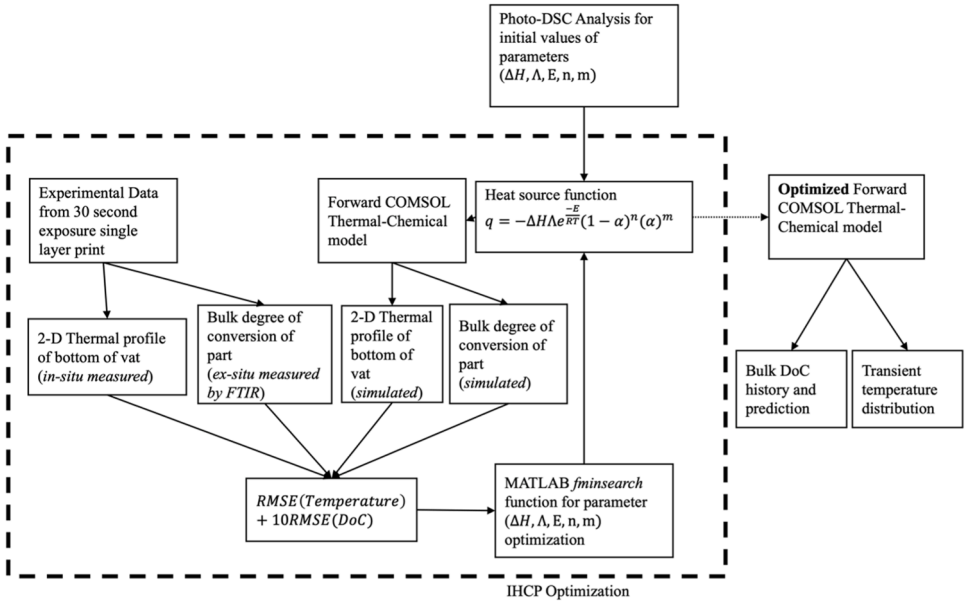

Fig. 5. Our developed IHCP optimization framework for thermal-chemical coupled modelling of a vat polymerization (VPP) process. This modelling approach compares the predictions of FEM simulation using the heat source estimated from a Photo-DSC guided chemical reaction heat generation model with the in-situ monitoring and ex-situ characterization results, thereby further optimizing the chemical heat source function until the comparison error is minimized.

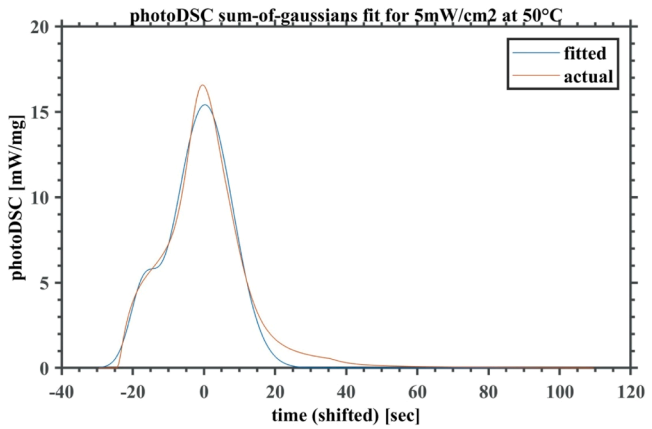

Fig. 6. Gaussian peak separation fitting of a sample Photo-DSC using the sum of two gaussian peaks.

reaction models, shown in Fig. 6. Namely, a data-driven model of the Photo-DSC characterization result is developed based on the works of Chen et al. and Zhang et al. [38,39]. Specifically, the autocatalytic reaction model, parameterized by temperature expressed in Eq. (4) (see Section 3.1), is used to fit the Photo-DSC results.

The fitted Photo-DSC model using the 5 mW/cm^2 photo-DSC dataset is shown in Table 1. The well-fitted reaction curves show that the autocatalytic model in Eq. (4) is appropriate for the model. However, the 10 mW/cm^2 was not used due to the fact that the peak resolution for the 40 C and 50 C DSC results were low and the peak separation yielding poor results. It is noted that the intensity levels used in the Photo-DSC characterization are not exactly the same as that used in the experimental printing. This is actually a common issue encountered in real VPP printing where light intensity could deviate from nominal light setting. Moreover, it is not practical for ex-situ characterization to experimentally characterize numerous levels of intensity that could be possibly used in VPP. As such, we want to examine the validity of the proposed method that even uses non-matching light exposures in Photo-DSC characterization. Furthermore, the intensity dependency is assumed to be absorbed by the pre-exponential Λ parameter, as shown in literature [40]. Besides, since the main purpose of the results extracted from this exercise is to be used as initial guesses for the IHCP optimization in Section 3.2, the most precise result of Photo-DSC is preferred but not required.

The fitted parameters are calculated using Matlab's *fitnlm* function as both the dependent and independent variables from Eq. (4) are given from the Photo-DSC results. A few further assumptions are made during the optimization from these results. Namely, the autocatalytic reaction is assumed to be nth order instead of nth/mth order as the n and m values are similar. Furthermore, the nth-order value is assumed to be the same from the fitting result.

4.2. Optimization of reaction rate parameters by using multi-reaction model and solving the IHCP

The vat substrate temperature evolution during and after the printing process is predicted by using COMSOL to simulate a FEM-based forward heat conduction model that has a heat source defined by two autocatalytic reaction models occurring simultaneously. The chemical reaction rate parameters of the two models are optimized by using an educated guess of initial values from Photo-DSC experiment data (Section 4.1) and solving the IHCP (Section 3.2).

To illustrate, as shown in Fig. 7, the time-varying distribution of vat substrate temperature is monitored in situ (Section 2.3) and predicted (Section 3.1) for a VPP process that undergoes 30-second exposure). The specific error minimization curve of predicted and in-situ measured vat substrate temperature is shown in Fig. A-2 in Appendix 2.

After iterations of IHCP optimization, the two autocatalytic reaction models are parameterized based on the values shown in Table 2. The initial values of A, ΔH, E are estimates as the fitting from Table 1 only provides $\Lambda e^{\frac{-E}{RT}}$, which is a function of the three variables, where $\Lambda = A\,\Delta H$. Instead, the initial values were selected to result in correct orders of magnitude for the final temperature readings as well as maintaining the proportion between the two reactions. The activation energy E is assumed to be the same for the two different reactions for the purpose of simplifying the problem. Although through literature the order of magnitude of the activation energy is similar for acrylic polymerization reactions [41], this is a major assumption that will need to be better examined in future works.

The enthalpy ΔH for the two peaks are 6.2 J kg^{-1} and 0.073 J kg^{-1}, reflecting the different reactions happening in this specific two-wavelength two-material curing process. The ability to estimate the enthalpy of different reactions will be very helpful in the further study of multi-wavelength multi-material VPP processes in the future as the variation in thermal signal due to the different magnitude of heat generation can help differentiate the different curing regions in multi-

Table 1
photo-DSC fitting results using auto-catalytic reaction model.

	Reaction 1	Reaction 2
$\Lambda e^{\frac{-E}{RT}}$ (s^{-1})	43.1	9.45
n	0.81	0.82
m	0.81	0.82

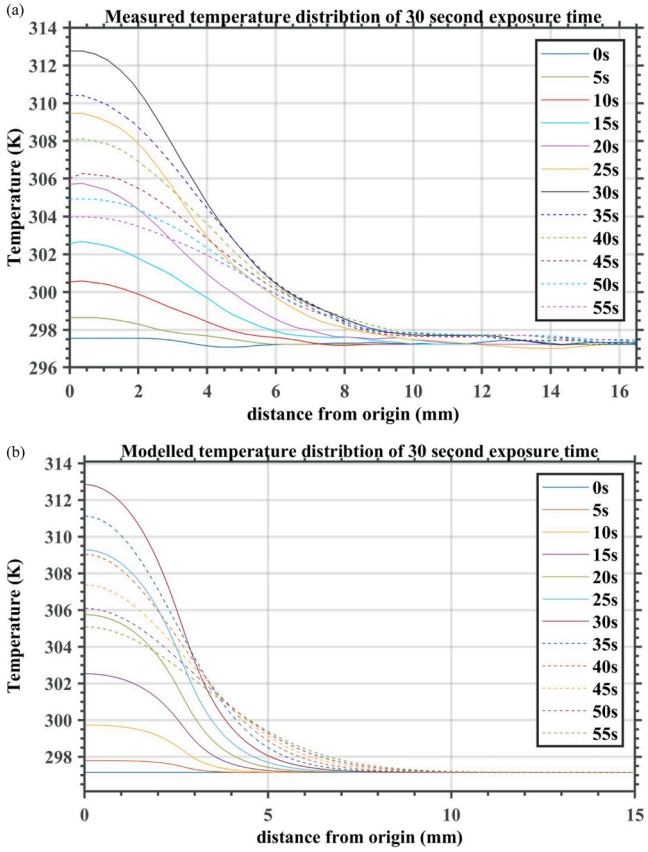

Fig. 7. Transient vat substrate temperature while curing a sample with an exposure duration of 30 second. Solid curves indicate the time points during the light curing, and dashed curves indicate the time points after turning off the light source (i.e., post printing). (a) In-situ measurement; (b) Prediction by simulating the optimized chemical reaction model.

Table 2
Optimized final reaction parameters for forward chemical reaction heat conduction prediction model.

x	Initial Value	Lower Bound	Upper Bound	Fitted Value
A_1 (s^{-1})	0.01	0	inf	0.0581
A_2 (s^{-1})	0.04	0	inf	0.238
ΔH_1 (J kg^{-1})	2	0	10	6.20
ΔH_2 (J kg^{-1})	0.1	0	10	0.073
E (J mol^{-1})	600	400	1000	557.6
n	0.81	0.5	2	0.50
m	$= n$	0.5	2	0.50

wavelength VPP processes. This creates a basis for potential future work.

4.3. Validation of optimized forward conduction model

Firstly, from Figs. 7(a) and 7(b), the optimized forward conduction model is shown to have thinner peaks from the central axis, and this can be attributed to the assumption of solid heat conduction that has been recognized as a major simplification of the model. The wider thermal distribution could also be a symptom of overcuring of the resin, as the final product is oft larger than the size of the light input. On the other hand, examining the transient temperature at the origin in Fig. 8, defined at the maximum temperature on the printer substrate, the model is found to be able to represent the temperature gradient due to the exothermic chemistry, which agrees with the in-situ thermal camera observation.

Furthermore, one can compare the work to that of literature. For example, the work of Emami et al. employs a free radical reaction model using significantly more parameters than this work presented, and operating at a level of abstraction that requires extensive property analysis for the correct parameters [20]. However, their results doesn't show significant improvement in terms of temperature prediction accuracy.

Using the post-IHCP optimized forward chemical reaction heat conduction model, we can interpolate and predict the degrees of cures at different time points during and after the printing process. The predicted bulk DoC, averaged across the curing region, is shown in Fig. 9.

The optimized model, as shown in Fig. 9, is adequate in interpolating the degree of cure history of the training sample, in this case samples at and less than the 30 s exposure used for the IHCP optimization. However, it overestimates the degree of cure predictions, as seen in the samples cured by light exposure for 40 and 50 second, thus showing that it is inadequate in extrapolation. However, it must be noted that the

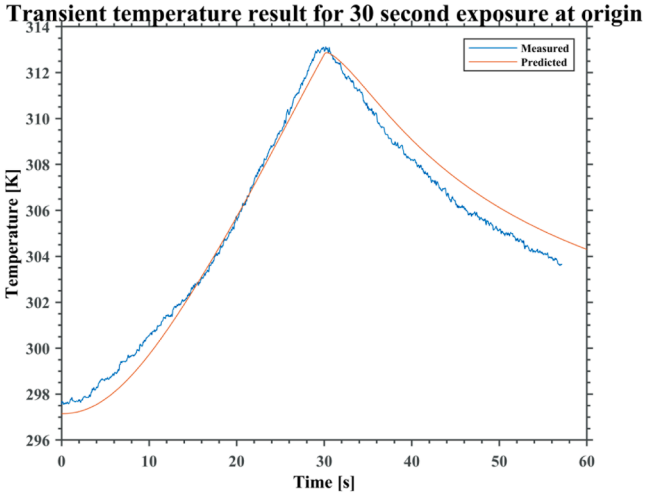

Fig. 8. Transient temperature at the center of the printed puck measured on the printer vat bottom (substrate) by in-situ thermal camera.

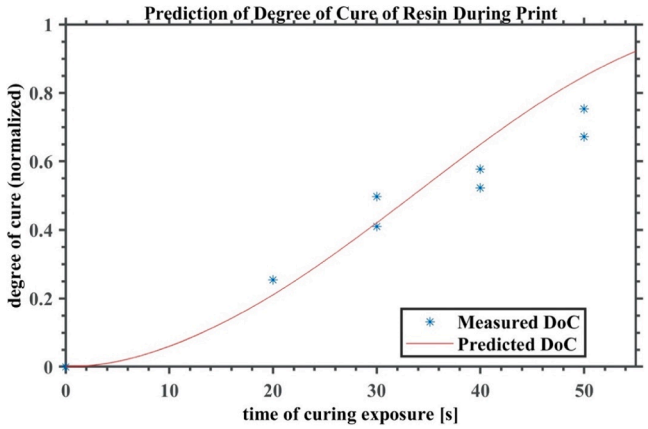

Fig. 9. Predicted Degree of Conversion using finite-element simulation of the heat conduction with optimized chemical reaction model.

reaction model used in the simulation is extremely simplified, selected primarily with the recognized low number of parameters as a benefit over accuracy. Further work should be done with more detailed photopolymerization models taken into account of the intensity component.

Secondarily, the temperature profile of curing zone is also an explorable output from the forward chemical reaction heat conduction model. Experimentally, however, it is difficult to validate the temperature profile in the active curing region of interest with ground truths. However, the thermally monitored region could be used as a surrogate for the accuracy of the predicted temperature profiles. The results of temperature are shown in Fig. 10. In step with the trend shown in Fig. 9, the predicted vat substrate temperature profiles are well fitted against the thermal history of the training sample, in this case the 0, 10, 20, and 30 second spatial distribution curves within a 50 second exposure time. Furthermore, the temperature predictions are lower than measured for the 40 and 50 second curves, as expected from the DoC prediction results. The overestimation of the DoC means that at the longer exposure times, the predicted reaction is closer to completion, and as such the exothermic heat generated is trending to zero earlier than the ground truth.

5. Conclusion

VPP process modeling should be accurate and robust, but it still faces challenges due to the severe lack of accurate results on the chemical reaction parameters and material properties. This challenge is heightened in the case of VPP processes that would like to adopt new material

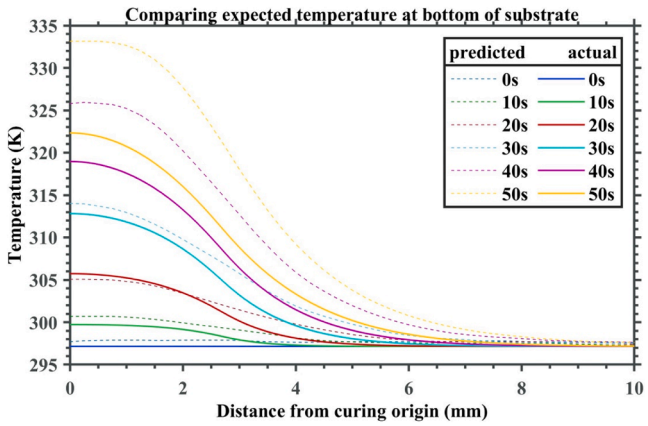

Fig. 10. Prediction of transient temperature distribution at bottom of the vat at exposure times during a 50 s exposure time print.

systems for novel products. It is unrealistic to use existent characterization methods to provide all the needed parameters for developing a comprehensive VPP process model. Nevertheless, limited ex-situ characterization joined by in-situ process monitoring can provide a good set of initial conditions and realistic processing dynamics to allow for a physics-informed data-driven thermal-chemical process modeling that help address the issue above. To this end, this work develops a new physics-based data-driven VPP process modeling method that couples the chemical reactions with thermal phenomenon. A thermal-chemical model of VPP is derived by optimizing a heat source equation that incorporates the degree of chemical conversion with an objective of minimizing the errors of DoC and temperature predicted by the following model approach. A forward thermal model with a chemical heat source that is educated by ex-situ Photo-DSC characterization experiment is optimized by applying an inverse-heat conduction approach that is informed by in-situ thermal monitoring. Specifically, an in-house DLP system with light projecting upwards through the vat is used to cure bulk samples with continuous exposures. The vat substrate temperature is measured using an in-situ infrared thermal camera and used as input to solve an IHCP for estimating the exothermic rate and the internal heat generation boundary conditions at the curing part. The estimated chemical heat source information is input to a forward FEM model that incorporates heat conduction and chemistry reaction. A lumped chemistry reaction equation that correlates DoC with heat is used as the chemistry model. The lumped chemistry model parameters are estimated by using Photo-DSC data as initial values, followed by an optimization that aims to minimize the errors between the model prediction and FTIR measurement of DoC values. In all, the developed framework of thermal-chemical modeling of VPP uses the in-situ monitoring-optimized IHCP forward solution, initialized with ex-situ photo-DSC results, to parameterize the heat source within the forward chemical-thermal FEM simulation of the VPP printing process. The model is validated by comparing the predicted DoC and vat substrate temperature against ex-situ FTIR and in-situ thermal camera measurements of printed parts at different exposure times. This new modelling method does not require exhaustive seeking for extensive model parameters and property values throughout literature or experiment. This allows the creation of models for more complex resin recipes that is a focus of research within VPP printing, especially with the rise in multi-wavelength printing. Further work can be done to apply the model to a realistic-printing scenario with additional layers and realistic layer thicknesses. Extensions of the work include moving away from the solid-material assumption, including the intensity dependency of the polymerization model, and applying the model to multi-layer printing.

CRediT authorship contribution statement

Heyang Zhang: Data curation, Formal analysis, Investigation, Methodology, Validation, Visualization, Writing – original draft. **Yue Zhang:** Formal analysis, Investigation, Methodology, Validation, Visualization, Writing – review & editing. **Xiayun Zhao:** Conceptualization, Funding acquisition, Investigation, Methodology, Project administration, Resources, Supervision, Writing – review & editing.

Declaration of competing interest

The authors declare that they have no known competing financial interests or personal relationships that could have appeared to influence the work reported in this paper.

Data availability

Data will be made available on request.

Acknowledgements

This material is based upon work supported by the National Science Foundation under Grant No. CMMI-2134447. Any opinions, findings, and conclusions or recommendations expressed in this publication are those of the authors and do not necessarily reflect the views of the National Science Foundation. The authors would like to thank Professor Minking K. Chyu for his generous sharing of their infrared thermal cameras as well as Dr. Yanxi Zhang for the Photo-DSC characterization work.

Appendix

A-1. Vat Photopolymerization Printing System

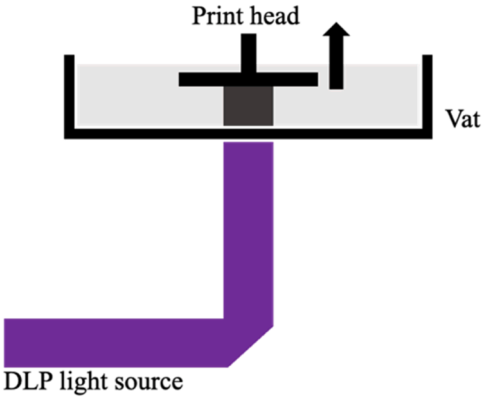

Fig. A-1. Representation of the DLP printer set-up.

Fig. A-1 shows the schematics of a typical DLP VPP printer, also the one used in this work. The DLP image is projected through the bottom of the resin chamber. The print starts with the build head inserting into the resin. After one layer is cured, the print head moves up by a specified layer thickness, and the void will be filled by the surrounding uncured resin and then a new layer is cured. This layer-by-layer process is repeated until the target 3D part is fabricated.

A-2. Optimization of the curing reaction model

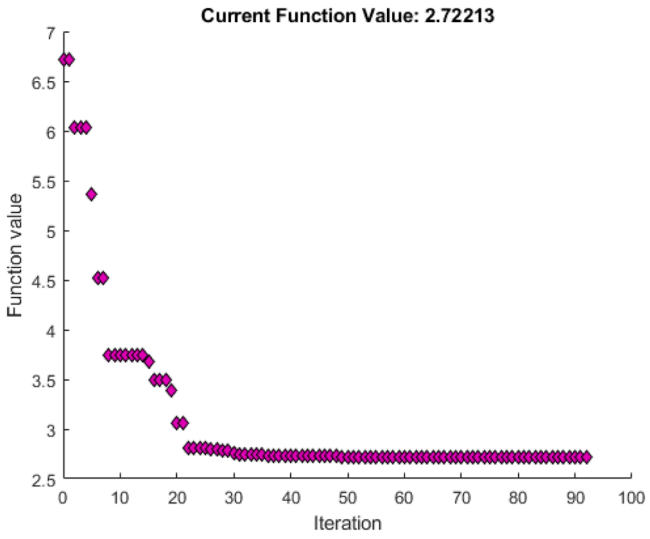

Fig. A-2. RMS Error minimization during optimization.

A-3. Raw Data of a samle FTIR measurement

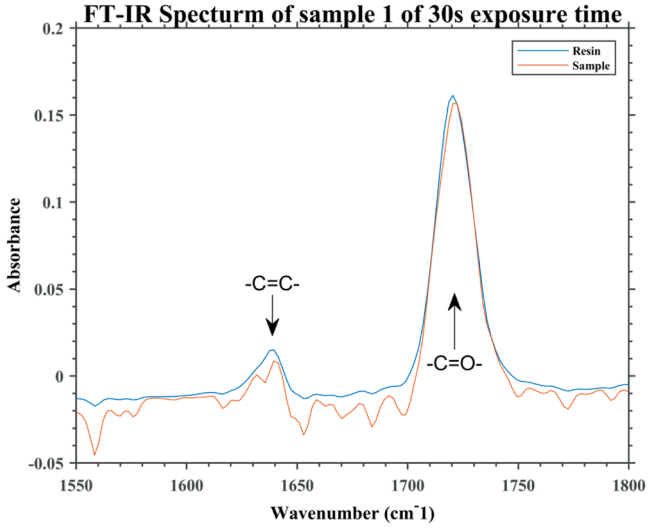

Fig. A-3. FT-IR data for a 30 s exposure time sample.

References

[1] S. Saleh Alghamdi, et al., Additive manufacturing of polymer materials: progress, promise and challenges, Polymers. (Basel) 13 (5) (2021).

[2] X. Kang, et al., Continuous 3D printing by controlling the curing degree of hybrid UV curing resin polymer, Polymer. (Guildf) (2021) 124284.

[3] C. Mendes-Felipe, et al., State-of-the-art and future challenges of uv curable polymer-based smart materials for printing technologies, Adv. Mater. Technol. (2019).

[4] J. Zhang, et al., Digital light processing based three-dimensional printing for medical applications, Int. J. Bioprint. 6 (1) (2020) 242.

[5] A. Nulty, 3D printing part 1: a history and literature review of 3D printing technologies used in dentistry, Dentistry J. (2021).

[6] M. Pagac, et al., A review of vat photopolymerization technology: materials, applications, challenges, and future trends of 3D printing, Polymers. (Basel) 13 (4) (2021).

[7] S.M. Montgomery, et al., Pixel-level grayscale manipulation to improve accuracy in digital light processing 3D printing, Adv. Funct. Mater. (2023) 2213252 **n/a**(n/a).

[8] X. Li, et al., 3D Printing Temporary Crown and Bridge by Temperature Controlled Mask Image Projection Stereolithography, Procedia Manuf. 26 (2018) 1023–1033.

[9] D.A. Walker, J.L. Hedrick, C.A. Mirkin, Rapid, large-volume, thermally controlled 3D printing using a mobile liquid interface, Science (1979) 366 (6463) (2019) 360–364.

[10] J.J. Schwartz, A.J. Boydston, Multimaterial actinic spatial control 3D and 4D printing, Nat. Commun. 10 (1) (2019) 791.

[11] Huang, S., et al., One-pot 3D printing of robust multimaterial devices. 2021.

[12] X. Zhang, et al., Wavelength-selective sequential polymer network formation controlled with a two-color responsive initiation system, Macromolecules 50 (15) (2017) 5652–5660.

[13] J. Hobich, et al., Synergistic, orthogonal, and antagonistic photochemistry for light-induced 3D printing, Macromol. Chem. Phys. (2022) 2200318.

[14] I. Cazin, et al., Spatially controlling the mechanical properties of 3D printed objects by dual-wavelength vat photopolymerization, Addit. Manuf. 57 (2022) 102977.

[15] J.W. Choi, et al., Sequential process optimization for a digital light processing system to minimize trial and error, Sci. Rep. 12 (1) (2022) 13553.

[16] M.D. Goodner, C.N. Bowman, Development of a comprehensive free radical photopolymerization model incorporating heat and mass transfer effects in thick films, Chem. Eng. Sci. 57 (5) (2002) 887–900.
[17] Z. Wu, et al., In situ monitoring of epoxy resin curing process: using glass transition as a bridge, Polym. Test. 117 (2023) 107871.
[18] T.H. Koen Classens, Steyn Westbeek, Joris J.C. Remmers, Siep Weiland, Multiphysical modeling and optimal control of material properties for photopolymerization processes, Sience 336 (2019) 4.
[19] S. Westbeek, et al., Prediction of the deformed geometry of vat photo-polymerized components using a multi-physical modeling framework, Addit. Manuf. 40 (2021) 101922.
[20] M.M. Emami, M. Jamshidian, D.W. Rosen, Multiphysics modeling and experiments of grayscale photopolymerization with application to microlens fabrication, J. Manuf. Sci. Eng. 143 (9) (2021).
[21] S.M. Montgomery, et al., A reaction–diffusion model for grayscale digital light processing 3D printing, Extreme Mech. Lett. 53 (2022) 101714.
[22] J. Bachmann, et al., Photo-differential scanning calorimetry parameter study of photopolymers used in digital light synthesis, SPE Polymers, 2021.
[23] F. Jiang, D. Drummer, Curing kinetic analysis of acrylate photopolymer for additive manufacturing by photo-DSC, Polymers. (Basel) 12 (5) (2020).
[24] M.C. Rusu, et al., Influence of temperature and UV intensity on photo-polymerization reaction studied by photo-DSC, J. Therm. Anal. Calorim. 110 (1) (2012) 287–294.
[25] M.I.B. Bernardi, et al., Thermal analysis and structural investigation of different dental composite resins, J. Therm. Anal. Calorim. 94 (3) (2008) 791–796.
[26] P.S. Elisabetta Cotti, Claudia Dettori, Guido Ennas, Comparison of the degree of conversion of resin based endodontic sealers using the DSC technique, Eur. J. Dent. 5 (April 2011) (2011).
[27] J. Bachmann, et al., Photo-differential scanning calorimetry parameter study of photopolymers used in digital light synthesis, SPE Polymers 3 (1) (2021) 41–53.
[28] J. Bachmann, et al., Investigation of the temperature influence on the dual curing urethane-methacrylate resin rigid polyurethane 70 (RPU 70) in digital light synthesis (DLS), Addit. Manuf. 37 (2021) 101677.
[29] J. Bachmann, et al., Photo-DSC method for liquid samples used in vat photopolymerization, Anal. Chim. Acta 1153 (2021) 338268.
[30] H. Zhang, X. Zhao, In-situ thermal monitoring informed modeling and simulation of process temperature during vat photopolymerization additive manufacturing, in: Materials Today: Proceedings, 2022.
[31] H. Zhang, C.K.P. Vallabh, X. Zhao, Registration and fusion of large-scale melt pool temperature and morphology monitoring data demonstrated for surface topography prediction in LPBF, Addit. Manuf. 58 (2022) 103075.
[32] B. JV, B. B, C.R. SC, Inverse heat conduction: ill-posed problems, Wiley, 1985.
[33] F. Zhu, et al., A deep learning method for estimating thermal boundary condition parameters in transient inverse heat transfer problem, Int. J. Heat. Mass Transf. 194 (2022) 123089.
[34] M. Raissi, P. Perdikaris, G.E. Karniadakis, Physics-informed neural networks: a deep learning framework for solving forward and inverse problems involving nonlinear partial differential equations, J. Comput. Phys. 378 (2019) 686–707.
[35] S. Cai, et al., Physics-informed neural networks for heat transfer problems, J. Heat. Transfer. 143 (6) (2021).
[36] W.J. Koros, J. Wang, R.M. Felder, Oxygen permeation through FEP Teflon and Kapton polyimide, J. Appl. Polym. Sci. 26 (8) (1981) 2805–2809.
[37] J. Humphry, et al., Isothermal differential scanning calorimetry analysis of the anionic polymerisation of polyamide-6: separation by dual asymmetric gaussians, Mater. Today Commun. 25 (2020).
[38] C. Chen, et al., An improved simplified approach for curing kinetics of epoxy resins by nonisothermal differential scanning calorimetry, High Perform. Poly. 30 (3) (2017) 303–311.
[39] C. Zhang, et al., Kinetic study of the novolac resin curing process using model fitting and model-free methods, Thermochimica. Acta 523 (2011) 63–69.
[40] K. Classens, et al., Multiphysical modeling and optimal control of material properties for photopolymerization processes, Addit. Manuf. 38 (2021).
[41] S. Hamzehlou, et al., Analyzing the discrepancies in the activation energies of the backbiting and β-scission reactions in the radical polymerization of n-butyl acrylate, Polym. Chem. 7 (11) (2016) 2069–2077.